AD-A157 934 AUTOMATIC DETECTION OF GULF STREAM RINGS(U) 1/1
MASSACHUSETTS UNIV AMHERST M F JANOWITZ JUN 85
TR-J8501 N00014-79-C-0629

UNCLASSIFIED F/G 17/5 NL

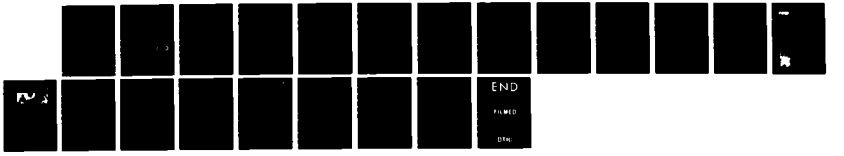

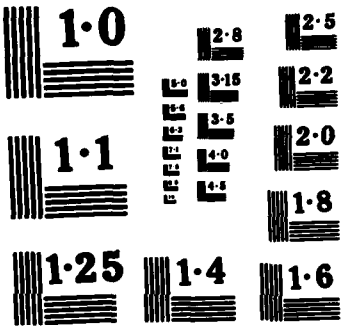

SECURITY CLASSIFICATION OF THIS PAGE (When Data Entered)

REPORT DOCUMENTATION PAGE		READ INSTRUCTIONS BEFORE COMPLETING FORM
1. REPORT NUMBER TR-J8501	2. GOVT ACCESSION NO.	3. RECIPIENT'S CATALOG NUMBER
4. TITLE (and Subtitle) AUTOMATIC DETECTION OF GULF STREAM RINGS		5. TYPE OF REPORT & PERIOD COVERED TECHNICAL Report MARCH, 1984 - JUNE, 1985 6. PERFORMING ORG. REPORT NUMBER
7. AUTHOR(s) M. F. JANOWITZ		8. CONTRACT OR GRANT NUMBER(s) N-00014-79-C-0629
9. PERFORMING ORGANIZATION NAME AND ADDRESS UNIVERSITY OF MASSACHUSETTS AMHERST, MA 01003		10. PROGRAM ELEMENT, PROJECT, TASK AREA & WORK UNIT NUMBERS 121405
11. CONTROLLING OFFICE NAME AND ADDRESS PROCURING CONTRACT OFFICER OFFICE OF NAVAL RESEARCH ARLINGTON, VA 22217		12. REPORT DATE JUNE, 1985 13. NUMBER OF PAGES 19
14. MONITORING AGENCY NAME & ADDRESS(if different from Controlling Office) OFFICE OF NAVAL RESEARCH, RESIDENT REPRESENTATIVE, HARVARD UNIVERSITY VANSBERG BLDG., ROOM 105, 29 Frances Avenue, Cambridge, MA 02138		15. SECURITY CLASS. (of this report) UNCLASSIFIED 15a. DECLASSIFICATION/DOWNGRADING SCHEDULE

16. DISTRIBUTION STATEMENT (of this Report)

APPROVED FOR PUBLIC RELEASE: DISTRIBUTION UNLIMITED

17. DISTRIBUTION STATEMENT (of the abstract entered in Block 20, if different from Report)

18. SUPPLEMENTARY NOTES

19. KEY WORDS (Continue on reverse side if necessary and identify by block number)

Gulf Stream rings, cold-core rings, warm-core rings, ellipse detection, digital images

20. ABSTRACT (Continue on reverse side if necessary and identify by block number)

A prototype for a program for the automatic detection of Gulf Stream rings from satellite IR images is described and illustrated. It includes a comparative study of 40 different filters on real data. The program involves a number of components: image smoothing, image simplification, edge detection, removal of small objects, and ellipse detection.

DD FORM 1 JAN 73 1473 EDITION OF 1 NOV 65 IS OBSOLETE
S/N 0102-014-6601

SECURITY CLASSIFICATION OF THIS PAGE (When Data Entered)

AUTOMATIC DETECTION OF GULF STREAM RINGS

M. F. Janowitz

1. Introduction. Cold-core rings are hydrographically distinguishable physical features that are spawned by meanders from the Gulf Stream. Typically, they are 150-300 km. in diameter, are roughly elliptical in shape and represent intrusions of cold water into the Sargasso Sea. Their boundary is similar to the South Wall of the Gulf Stream. The meandering process is described in [5], [8] and [12], with studies of cold-core rings appearing, among other places, in [14] and [17]. Warm-core rings form in the slope water region between the Gulf Stream and the North Atlantic Continental Shelf ([7], [15]). They too are roughly elliptical in shape with a diameter of 100-200 km.; a warm-core ring boundary consists of water similar to the North Wall of the Gulf Stream. Several satellite studies of Gulf Stream rings have been made. Among them are [1], [2], [9] and [16]. It should be noted though that the location of ring centers from satellite IR imagery is by no means a simple task. Substantial portions of ring boundaries are often obscured by clouds, and though the rings themselves tend to be elliptical in shape, there is some variation and fuzziness in their boundaries as well as some axial asymmetry. This has been observed in several studies ([1], [3], [4] and [11] among others). In [1] a technique is described for locating ring boundaries from digital IR satellite images. It involves an analyst moving a cursor over the boundary and recording coordinates of the resulting points. A least squares fit is then provided to a curve of the form

$$ax^2 + 2hxy + by^2 + 2gx + 2fy + c = 0$$

with $h^2 < ab$. From this, the center and orientation of the ring can be estimated.

Our goal in the present report is somewhat different. A prototype for the automatic detection of Gulf Stream rings will be described and illustrated. A sequence of techniques are employed, and these are individually described in §2:

A. Image smoothing and cloud removal.

B. Image simplification.

C. Edge detection.

D. Removal of objects of the wrong size.

E. Ellipse detection.

Once a ring has been located, more sophisticated techniques may be employed to determine its center and orientation. Finally, in §3, the techniques will be applied to some data furnished by NAVOCEANO, Code 9110. The image shows 3 cold-core rings, and comes from AVHRR Band 4 of Orbit 9520 of NOAA-7 (28 April, 1983).

2. Description of Algorithms. Corresponding to the 5 algorithms defined at the end of §1, the section will be broken into 5 parts.

A. Image smoothing and cloud removal. The cloud removal techniques will be described elsewhere, so let us simply assume that we are dealing with a cloud free image. Preliminary image smoothing is accomplished by 2 iterations of a spatial 3 by 3 filter. A total of 40 such filters was tried, and our goal here will be to describe them. This will be done in stages, as the filters themselves fall into roughly 3 different categories. The first category represents variations of a median and mean filter, and here they are:

Filter No.	Description
1	Median
2	Trimmed Mean. Remove highest and lowest value, and take mean of those remaining.
3	Trimmed mean, removing highest and lowest two values.
4	Lowest value in window
5	Third from bottom value
6	Seventh from bottom value
7	Highest value in window
8	Mean of 3 lowest values
9	Mean of 5 lowest values
10	Mean of 7 lowest values
11	Mean of 3 highest values
12	Mean of 5 highest values
13	Mean of 7 highest values
14	Straight 3 by 3 mean

The second category of filters has its genesis in a paper by Narayanan and Rosenfield [10]. The idea behind their operation is both simple and powerful. Suppose that a digital image contains grey levels in the range from IMIN to IMAX. Suppose further that some statistic $S(I)$ is associated with each grey level I, and that $S(I) \leq S(J)$ implies that grey level J is somehow more reliable than grey level I. Though there are other possibilities, one might think of $S(I)$ as being the frequency count of I. Suppose the center pixel of a 3 by 3 neighborhood has grey level I. Rather than take a straight mean of the pixels in the neighborhood, one selects only those pixels that are in some sense more likely to have a correct grey level than does the center pixel. Method 1a averages in those pixels whose grey level J is such that $S(J) \geq S(I)$; method 1c wants $S(J) \geq S(I)$ and $|J - I| \leq 2$. Method 1b coincides with 1a, and 1d with

1c, except that if fewer than 3 pixels are to be averaged, then the center pixel is deemed noise, and the filter output becomes the mean of the 3 by 3 neighborhood with the center pixel removed. Method 2a is like 1a, except that no peak $S(k)$ is allowed with k between i and j, while 2c is like 1a with at most 2 peaks allowed for values between i and j. Methods 2b and 2d are the analogues of 1b and 1d. With $S(I)$ representing the frequency count of level I, we now have:

Filter No.	Description
15	Method 1a
16	Method 1b
17	Method 1c
18	Method 1d
19	Method 2a
20	Method 2b
21	Method 2c
22	Method 2d

Two other choices for the statistic S were tried. Option B used the negative of the average standard deviation of 3 by 3 neighborhoods centered on pixels having grey level I, while option C represented the empirical probability that a pixel that was a neighbor of a pixel with grey level I would itself have grey level I (a careful description of this statistic occurs in [6]). With this scheme, the frequency count definition for S could be called option A. We summarize options B and C in a single table.

Option B Filter No.	Option C Filter No.	Description
23	31	Method 1a
24	32	Method 1b
25	33	Method 1c
26	34	Method 1d
27	35	Method 2a
28	36	Method 2b
29	37	Method 2c
30	38	Method 2d

The remaining two filters are modifications of a median filter. In each case, a 3 by 3 neighborhood is rank ordered by grey level, with the highest grey level given rank 1. Filter Number 39 outputs the rank 4 value if the center pixel rank ≥ 4, the rank 6 value if the center pixel rank ≤ 6, and the median if the center pixel rank is 5. Filter Number 40 outputs the median if the center pixel rank is not 4, 5 or 6, and otherwise leaves the center pixel unchanged.

B. Image simplification. Even after two applications of a smoothing filter, an image will usually be too noisy to effectively locate edges of Gulf Stream rings. A single pass of a suitable image simplification algorithm will serve to rectify this problem. A careful and detailed description of this algorithm occurs in [6], so we shall be content with a brief summary of its operation. The input to the algorithm consists of the original image ORIG and a filtered version FIL. Two statistics are calculated. S(I) is the statistic for grey level I that was used in Option C of the filters, and it is computed on FIL. Further, for each grey level of I of FIL, one computes the mean M(I) of all those pixels in ORIG whose filtered version in FIL has grey level I. The grey levels are rank ordered by S(I) to form a sequence $I_1, I_2, \ldots, I_k$ with

$S(I_1) \leq S(I_2) \leq \ldots \leq S(I_k)$. A list of levels to be deleted is now constructed:

I_1 is always deleted.

I_j is deleted provided neither $I_j - 1$ nor $I_j + 1$ has already been deleted.

This guarantees that adjacent grey levels are never simultaneously deleted, so at most half of the grey levels in an image are deleted. Pixels in a deleted grey level I are assigned to that remaining level J that minimizes $|M(I) - M(J)|$.

C. Edge Detection. A Kirsch edge detector (as described in [13]) is employed. Its output is then thresholded so as to produce a binary edge image. Identical thresholds were used for the various filter options.

D. Object Removal. As a further step toward image simplification, any object that is too small to be a ring is removed. The algorithm passes a k by k window over the picture. If the outer edge of the window contains no edge elements, then the edge elements within the window are removed. A suitable choice for k will leave any ring boundaries unchanged, and yet remove much of the background clutter that is too small to be a ring.

E. Ellipse Detection. A k by k window (k an odd integer) is passed over the binary edge output that results from applying C and D. At each position of the window the center pixel is tested to see if it could be the center of an ellipse lying within the window. Using polar

coordinates with the center pixel as the origin, the rays $\theta_i = 2\pi i/t$ $(i = 0,1,\ldots,t-1)$ are now produced and the distances d_i recorded where the first edge element along θ_i is found, with $d_i = 0$ if no edge elements are encountered within the window. If t is an even integer, then one may use opposite rays to locate a major axis for any potential ellipse. The minor axis is then chosen to be the pair of rays that are perpendicular to this major axis, provided their "d" values are not 0. Otherwise, one can look at diameters close to the perpendicular to find the length of the minor axis. If no minor axis can be calculated, the process stops and an error message results. Assuming that a major and minor axis have been calculated, one now simply predicts where each ray θ_i should hit an edge, and computes the sum of the differences between the observed and calculated values. Near an ellipse center this error sum has a dramatic dropoff, and preliminary work shows that it is possible to set a threshold that will allow an effective decision to be made as to whether the center pixel is indeed the center of an ellipse. To compensate for errors in digitization, and the fact that we are looking at a low resolution version of a picture, it is often useful to do the above process with d_i replaced by $\max(0,d_i - \sqrt{2}/2)$. Because of the nature of the algorithm, it is convenient to represent an ellipse in polar coordinates, centered on the center pixel. The equation

$$b^2x^2 + a^2y^2 = a^2b^2$$

then becomes

$$r^2b^2\cos^2\theta + r^2a^2\sin^2\theta = a^2b^2$$

and after some routine algebraic manipulation, one finds that

$$r^2 = b^2/\left(1 + \left(\frac{b^2}{a^2} - 1\right)\cos^2\theta\right).$$

A lookup table of values of $\cos^2\theta$ now allows for the rapid calculation of values of r.

Though this is the technique on which the paper is based, it is by no means the only method that was tried. If one wishes to allow for axial asymmetry, for example, one can fit 4 sections of ellipses together by joining them at the vertices. There are also other candidates for errors. One can use the predicted y-value of an ellipse instead of predicted ray lengths as a means of measuring error in fit.

3. Applications to Real Data. The algorithms were tested on the image described on p. 2. A portion of this image is displayed in Figure 1, and it contains 3 cold-core rings. The algorithms were actually applied to the image displayed at the top of Figure 2. This represents a subimage of Figure 1 containing the rings. This subimage was reduced by a factor of 2 in both the horizontal and vertical directions, so that what is displayed contains 84 rows and 139 columns. The bottom image of Figure 2 is the output of a Kirsch edge detector on the top image. It illustrates the need for some image smoothing and image simplification before any attempt can be made to detect elliptical objects. Figures 3-7 contain the final output corresponding to each of the 40 filter techniques. The 9 images in Figure 3 represent the outputs of

Filter 1	Filter 2	Filter 3	(Row 1)
Filter 4	Filter 5	Filter 6	(Row 2)
Filter 7	Filter 8	Filter 9	(Row 3)

In a similar fashion, Figure 4 depicts Filters 10-18, Figure 5 Filters 19-27, Figure 6 Filters 28-36, while Figure 7 contains Filters 37-40.

Though it is clear that no conclusions may be drawn from a single image, one can still observe that the most promising filters are: 1,2,3,14,15,16,17,18,19,20,21,22 and 40. These filters represent mean filters, trimmed means, medians, and the global information filters proposed in [10]. Much more work needs to be done before any meaningful conclusions can be drawn. Changes in thresholding of the filtered images, for example, will produce dramatic differences in the final output, as will modifications of the image simplification algorithm. Even so, when the ellipse detection algorithm is applied to images such as those that resulted from Filters 1,2 or 3, the result was the correct detection of the 3 cold-core rings with no false ring detections of any kind. To illustrate this, we present the results obtained by applying the ellipse detector to the output of Filter 1. The program used rays in a 43 by 43 window centered on alternate rows and columns. The goodness-of-fit statistic was computed only if the program decided that the center pixel was not close to an edge point, and that a sufficient number of rays intersected edge points. A total of 24 rays were used for the following data, but similar results were obtained using only 16 rays. The program correctly detected centers of rings at positions (35,82), (60,116), and (62,35), where the symbol (I,J) denotes the I-th row from the bottom and the J-th column from the right of the image.

Row Number	Column Number	Statistic
24	78	.26
26	88	.18
26	90	.31
28	90	.13
30	82	.25
32	80	.14
32	82	.05
32	84	.16
34	80	.11
34	82	.01
34	84	.09
36	80	.14
36	82	.01
36	84	.06
38	82	.07
38	84	.11
38	118	.13
54	26	.31
60	30	.14
60	32	.07
60	34	.05
60	36	.06
60	38	.12
60	110	.25
60	114	.06
60	116	.03
60	118	.09
62	30	.13
60	32	.04
62	34	.01
62	36	.01
62	38	.07
62	40	.14
62	116	.06

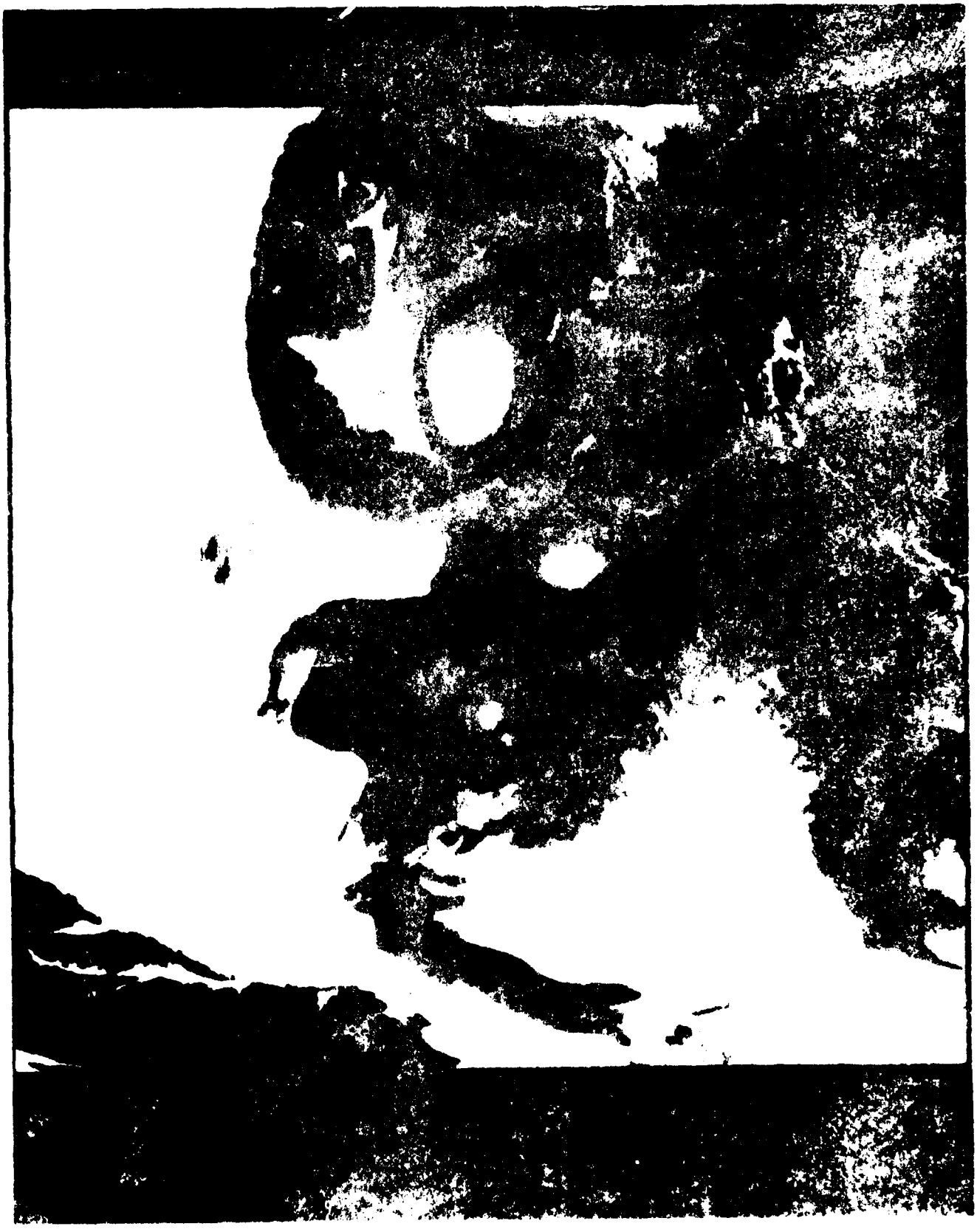

Fig. 1. Portion of Orbit 0[illegible] NOAA-7 of 28 April. 1983

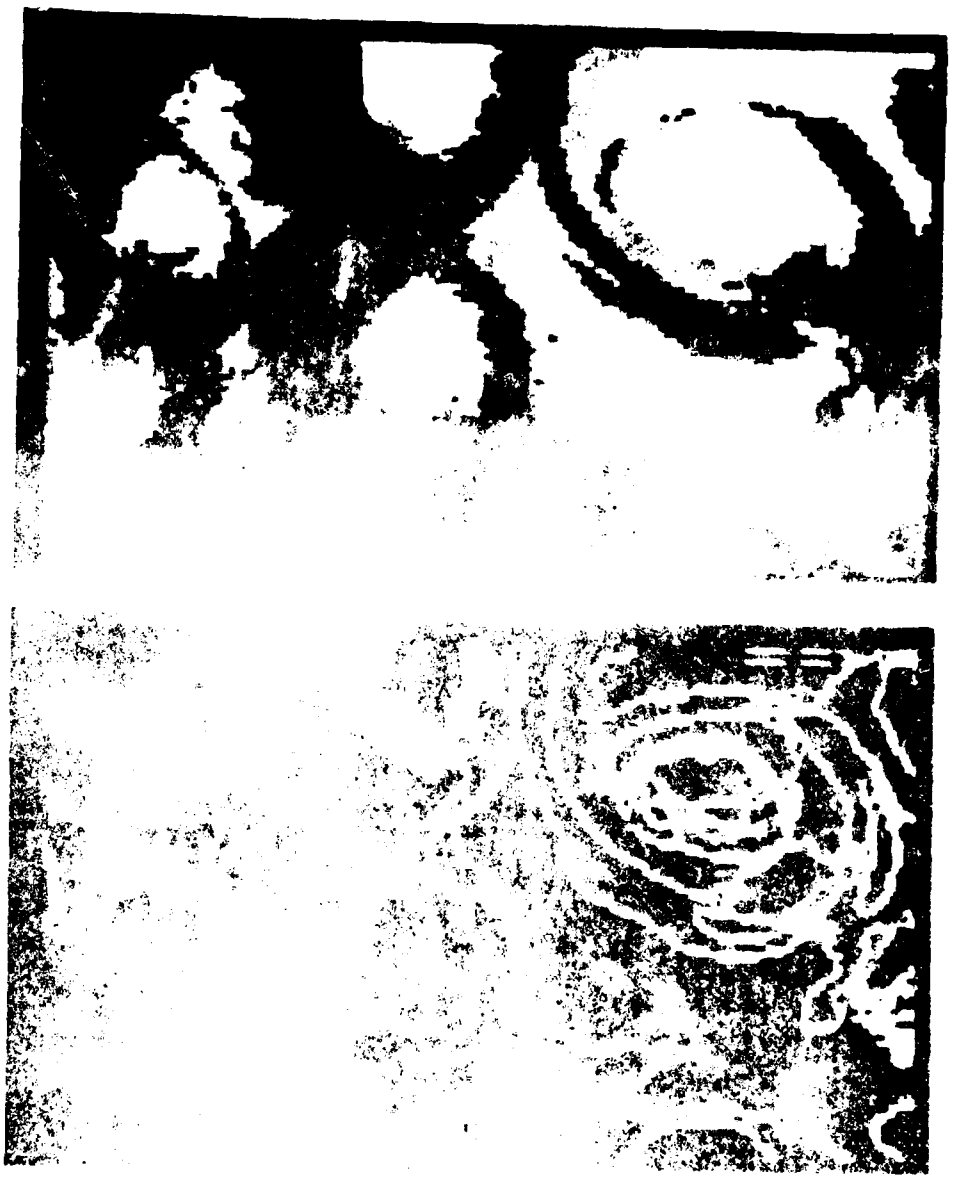

Fig. [illegible] tion reduced by a factor
[illegible] (Top)
[illegible] tom)

Fig. 3. Filter 1-9 (See text for explanation)

Fig. 4 Filters 10-18 (See test for explanation)

(See next for explanation)

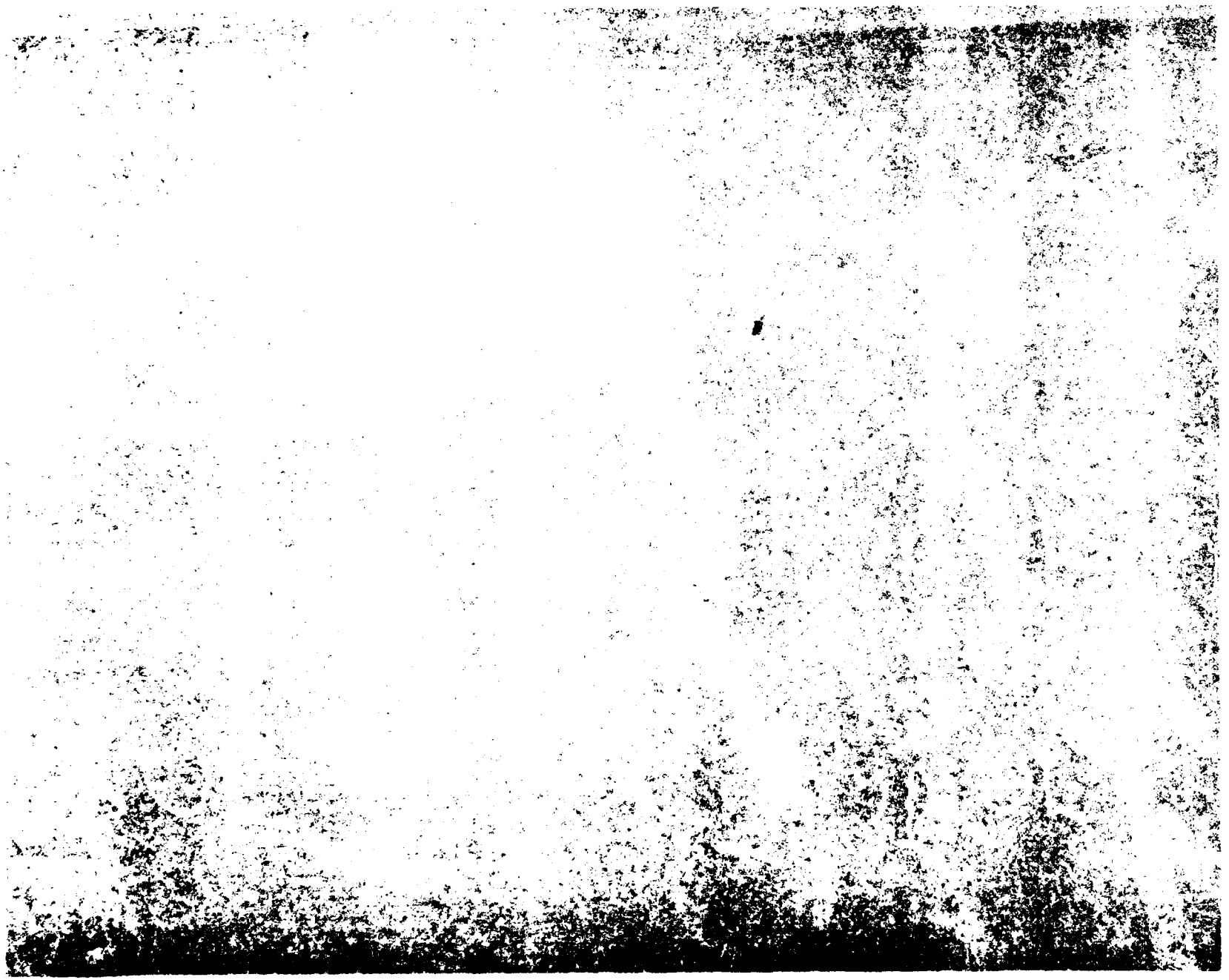

Fig. 6. Filters 28-36 (See text for explanation)

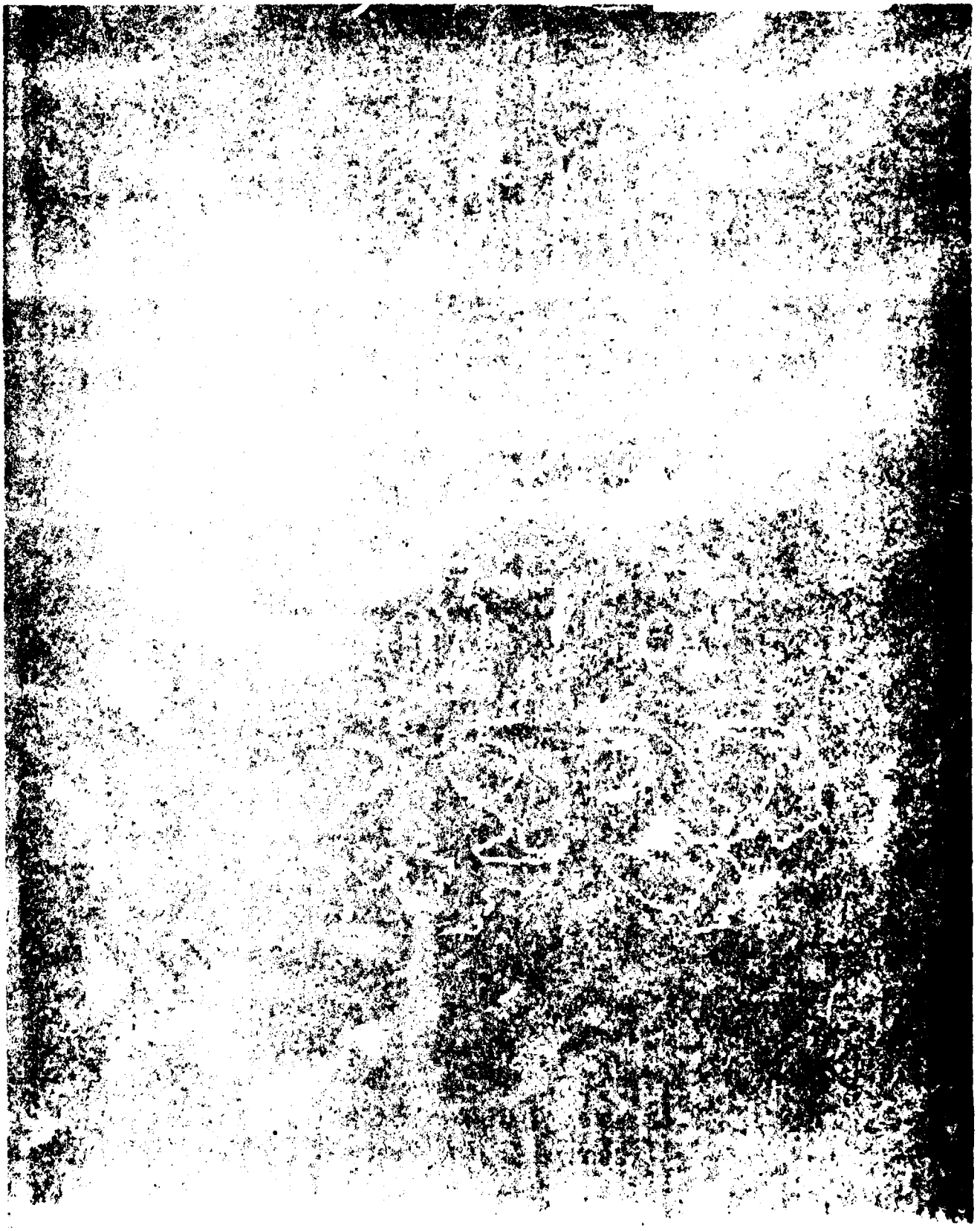

Fig. 7. Filters 37-40 (See text for explanation)

REFERENCES

[1] Brown, O.B., Olson, D. B., Brown, J.B., and Evans, R. H., Satellite Infrared Observation of the Kinematics of a Warm-Core Ring, Aust. J. Mar. Freshw. Res. 34 (1983), 535-545.

[2] Brown, O.B., and Evans, R. H., Satellite visible and infrared remote sensing: a status report, Nav. Res. Rev., Winter 1981, 1 (1982) 7-25.

[3] Cheney, R.E., Gemmill, W.H., Shank, M.K., Richardson, P.L. and Webb, D., Tracking a Gulf Stream ring with SOFAR floats, J. Phys. Ocean. 7 (1976),

[4] Flierl, G. R., The application of linear quasigeostrophic dynamics to Gulf Stream rings, J. Phys. Ocean, 7 (1977) 365-379.

[5] Fuglister, F.C., Cyclonic rings formed by the Gulf Stream, 1965-66. In "Studies in Physical Oceanography. A tribute to George Wurst on his 80th birthday". (Ed. A.L. Gordon.) Vol. 1, 137-168 (1972), Gordon and Breach, New York.

[6] Janowitz, M.F., A cluster analysis program for image segmentation. In "Statistical Signal Processing". (Ed. E.J. Wegman and J.G. Smith), 399-410, Dekker, New York (1984).

[7] Joyce, T.M., Schmitt, R.W., and Stalcup, M.C., Influence of the Gulf Stream upon the short-term evolution of a warm-core ring, Aust. J. Mar. Freshw. Res., 34 (1983), 515-524.

[8] Lai, D. and Richardson, P., Distribution and movement of Gulf Stream rings, J. Phys. Ocean. 7 (1977), 670-683.

[9] Mizenko, D. and Chamberlin, J., Anticyclonic Gulf Stream eddies off the northeastern United States during 1976, Ann. Biol. 34 (1979), 39-44.

[10] Narayanan, K. A. and Rosenfield, A., Image smoothing by local use of global information, IEEE Trans. on Syst., Man and Cyber, SMC-11 (1981), 826-831.

[11] Olson, D. B. and Spence, T.W., Asymmetric disturbances in the frontal zone of a Gulf Stream ring, J. Geophys. Res. 83 (1978), 4691-95.

!12] Parker, C.E., Gulf Stream rings in the Sargasso Sea, Deep SEa Res. 18 (1971), 981-93.

[13] Pratt, W. K., Digital Image Processing, Wiley, New York, 1978.

[14] Ring Group, Gulf Stream cold-core rings: their physics, chemistry and biology, Science 212 (1981), 1091-1100.

[15] Saunders, P.M., Anticyclonic eddies formed by shoreward meanders of the Gulf Stream, Deep Sea Res., 18 (1971), 1207-19.

[16] Spence, T. W. and Legeskis, R., Satellite and hydrographic observations of low-frequency wave motions associated with a cold-core Gulf Stream ring, J. Geophys. Res. 86 (1978), 1945-54.

[17] Wiebe, P. H. and Flierl, G.R., Euphausiid invasion/dispersal in Gulf Stream cold-core rings, Aust. J. Mar. Freshw. Res., 34 (1983), 625-652.

END

FILMED

9-85

DTIC